A new scenario applying traffic flow analogy to poleward expansion of auroras

Osuke Saka

Office Geophysik, Ogoori, Japan

Abstract

Transient westward electric fields from the magnetosphere generate equatorward plasma drifts of the order of kilometers per second in the auroral ionosphere. This flow channel extends in north-south directions and is produced in the initial pulse of Pi2 pulsations. Drifts in the ionosphere of the order of kilometers per second that accumulated plasmas at the low latitude end of the flow channel are of such large degree that possible vertical transport effects (including precipitation) along the field lines may be ignored. In order to interrupt the excess accumulation through the drift, we suggest that ionosphere responds nonlinearly to decelerate the equatorward drifts in the flow channel analogous to a traffic flow of cars on crowded roads. We apply this analogy to the poleward expansion of auroras.

1. Introduction

"Auroras and solar corona observed at the solar eclipse are optical phenomena unique in space physics. With enough knowledge about the underlying physical processes, once auroras have been captured by a highly sensitive imager, they provide an unexpected wealth of information about plasma environment of the Earth" [Oguti, 2010]. Plasma drifts in the ionosphere observed by the balloon-measured electric fields [Kelley et al., 1971], by the Ba releases [Haerendel, 1972] and by radar observations [Nielsen and Greenwald, 1978] did not match the expanding trajectories of auroras. This fact raises one of several unanswered questions involving violent poleward motion of auroras [Akasofu et al., 1966]. To account for the difference in propagation directions, it was suggested that auroras were directly connected to the reconnecting flux tube moving tailward in the plasma sheet. This idea suggests that the primary sources of particles are in the magnetosphere, though they might be accelerated in lower altitudes for precipitations. This concept has been accepted in the literature for many decades.

It is worthy to consider whether the above idea also explains auroras associated with Pi2 pulsations. This is because Pi2 pulsations are accompanied by non-vortical slippage motions in the equatorial plane of midnight magnetosphere [Saka et al., 2007] while plasma motions in the auroral ionosphere were dominated by vortical flows [Saka et al., 2015]. The third harmonic deformations of the geomagnetic fields were generated in the midnight magnetosphere for tying two regions between slippage motions in the magnetosphere and vortical motions in the auroral ionosphere [Saka et al., 2012]. We may thus infer that vortical flows in the ionosphere do not originate in the magnetosphere but are rather generated in the ionosphere itself [Saka et al., 2012]. In this context, we interpret the motion of auroras as of ionospheric origin.

2. Auroras and field line reconfigurations associated with Pi2

In Pi2 pulsations, poleward expansion of auroras arising out of the onset arc was observed in the initial pulse of Pi2 pulsations [Saka et al., 2012]. Statistical study of geomagnetic fields at geosynchronous orbit during Pi2 showed that field line inclination at geosynchronous orbit (Goes5/6 at 285°/252° in geographic coordinates) decreased continuously in the growth phase and attained 33.6°/49.4° in dipole coordinates 2-min prior to the initial peak of Pi2 amplitudes [Saka et al., 2010]. This result suggests the observed field line inclination prior to the onset conforms to T89 model of Kp=4 [Tsyganenko, 1989]. These field lines were mapped to auroral ionosphere at 63.4°N/62.7°N in geomagnetic coordinates corresponding to a latitude of onset arc. From these estimations, we suggest that Bursty Bulk Flows (BBFs) appeared first at the onset latitudes and activated preonset auroras. In the initial pulse of Pi2 pulsations, field line inclination of Goes5 increased in a step-like manner, while for Goes6 transient pulses were observed [Saka et al., 2010]. The average latitudes of Goes5 and Goes6 were at 10.3°N and 7.9°N, respectively in the T89 model for the average Kp index of 3. It is likely that dipolarization was composed of transient pulses at latitudes closer to the equatorial plane. In the following Pi2 pulses, an auroral surge was observed in all-sky images between 66°N to 74°N in geomagnetic latitudes. They propagated eastward or westward at the poleward boundary of the auroral zone and were interpreted as an auroral manifestation of flow bifurcation of fast earthward flows (BBFs) [Saka et al., 2012].

Simultaneous with reconfigurations of field lines in meridional plane, field lines stretching initially in tailward directions switched to dawn-dusk directions in the initial pulse of Pi2s [Saka et al., 2000]. This switching was associated with the excitation of slow MHD wave by the increasing inflows of plasma sheet ions toward the equatorial plane in growth phase [Saka and Hayashi, 2017]. After manipulating a set of linearized MHD equations [Kadomtsev, 1976], we have a relation between parallel shrinkage of plasmas along the field lines (ξ_z) and perpendicular stretching of the field lines ($\xi_\perp$) in the following form,

$$\xi_z = \frac{C_S^2}{\omega^2} F \cdot B_0^2 \frac{\partial}{\partial z}(div\xi_\perp) . \qquad (1)$$

Here, C_s, ω and B_0 are the sound velocity, angular frequency of waves and background field magnitudes, respectively. F is given by $F = \frac{C_A^2}{B_0^2}\frac{1}{C_s^2 - (\frac{\omega}{k})^2}$ and is positive for the slow mode and negative for the fast mode. C_A denotes Alfven velocity. If the wave mode was the fast mode, flux tubes would have contracted in longitudes towards the midnight sector, which was not observed during the first one-minute-interval of Pi2 onset (initial pulse of Pi2 onset). An alternative explanation of polarization switching may involve Ballooning instability of the coupled poloidal Alfven and slow magnetoacoustic modes [Rubtsov et al., 2018]. This switching from tailward to dawn-dusk directions disrupts the cross-tail currents creating a step like dipolarization or dipolarization pulses in the initial pulse of Pi2 pulsations and producing transient convection surge and associated westward electric fields in the midnight sector. The convection surge occurred once in the initial pulse of Pi2 pulsation but is not repeated in the following pulses.

3. Horizontal plasma flows in the ionosphere

It is reasonable to assume that westward electric fields were transmitted along the field lines to the auroral ionosphere by the guided poloidal mode [Radoski, 1967] from the surge location and created an equatorward flow through $E \times B$ drift of the order of kilometers per second in the auroral ionosphere. Electric fields of the order of 100 mV/m generate these high velocity flows in the ionosphere. The flows would be confined in a channel expanding in the north-south directions in the midnight sector. The low-latitude end of the flow channel was at the latitudes of the onset arc corresponding to earthward edge of the BBFs. The high-latitude end may not expand beyond the poleward boundary of auroral zone. Longitudinal width of the flow channel may be in about 1 to 2 hours of local time (~1000 km along 65°N) corresponding to horizontal scale size of Pi2 vortices [Saka et al., 2014].

In the flow channel, drift across the magnetic fields for the *j-th* species ($\mathbf{U}_{j\perp}$) can be written in the F region as [Kelley, 1989],

$$\mathbf{U}_{j\perp} = \frac{1}{B}[\mathbf{E} - \frac{k_B T_j}{q_j} \frac{\nabla n}{n}] \times \hat{\mathbf{B}} . \qquad (2)$$

Here, $\mathbf{E}$ denote westward electric fields in the flow channel and $\hat{\mathbf{B}}$ denotes a unit vector of the magnetic fields B, downward in the auroral ionosphere. Symbols k_B, T_j, q_j, and n are the Boltzmann constant, temperature of the *j-th* species, charge of the *j-th* species, and density of electrons (ions), respectively. The electric field of the order of 100 mV/m exceeded the diffusion (second term) by three orders of magnitudes in low temperature ionosphere. The $E \times B$ drift predominated in the F region and diffusion term may be ignored. In the E region, drift trajectories may be written [Kelley, 1989] for electrons by,

$$\mathbf{U}_{e\perp} = \frac{1}{B}[\mathbf{E} \times \hat{\mathbf{B}}] \qquad (3)$$

and for ions by,

$$\mathbf{U}_{i\perp} = b_i[\mathbf{E} + \kappa_i \mathbf{E} \times \hat{\mathbf{B}}]. \qquad (4)$$

Here, b_i is mobility of ions defined as $\Omega_i/(B\nu_{in})$, κ_i is defined as Ω_i/ν_{in}. Symbols Ω_i and ν_{in} are ion gyrofrequency and ion-neutral collision frequency, respectively. $\hat{\mathbf{B}}$ denotes a unit vector of the magnetic fields B. To derive equations (3) and (4), pressure gradient term (diffusion) was again ignored. In the E region ($\kappa_i = 0.1$), although the first term of (4) exceeds the second term by one order of magnitudes, plasma accumulation in equatorward latitudes by the imposed westward electric fields was produced by equation (3) for electrons and the second term in (4) for ions. However, electron accumulation in lower latitudes increased southward electric fields and simultaneously ion drifts in the first term of (4). If the southward electric fields grew to exceed the westward electric fields by an order of magnitudes, ion drifts in the first term of (4) and electron drifts in (3) balanced to satisfy the quasi-neutrality. This is equivalent to the generation of the Pedersen currents in the ionosphere. Thus, electrostatic potential is generated in the E region, positive in poleward and negative in equatorward. The Pedersen currents would have closed to the field-aligned current (FAC) and sustain the steady state electrostatic potential produced in the ionosphere. Plasma drifts in the ionosphere, both in E and F regions, accumulate density at the low-latitude edge of the flow channel. In the following section, we discuss vertical transport of these accumulated materials from the low-latitude edge of the flow channel.

4. Vertical plasma flows in the ionosphere

The transient compression of the ionospheric plasmas at the low-latitude edge of flow channel would excite the ion acoustic wave in the ionosphere travelling along the field lines upward and downward directions from the density peak of the F region. Figure 1 shows altitude distribution of the pre-onset density profile of electrons (black) and density profile caused by the accumulation in red. The accumulation doubled the electron density profile from 90 km to 1000 km in altitudes. Electron density profile in black was plotted using sunspot maximum condition given in Prince and Bostic (1964). The travelling ion acoustic waves, upward and downward, are denoted by vertical arrows. Ion acoustic wave propagating downward may be eventually absorbed in the neutrals, while the upward wave may propagate along the field lines further upward. We will focus only on the upward travelling ion acoustic wave. The ion acoustic wave produced the parallel electric fields in accordance with the Boltzmann relation [Chen, 1974],

$$E_{//} = -\frac{k_B T_e}{q}\frac{\nabla_{//} n_e}{n_e}. \qquad (5)$$

Here, k_B is Boltzmann constant, q is electron charge, T_e is electron temperature, and n_e is electron density ($n_e = n_i$). Equation (5) gives electric field strengths of the order of $0.4\mu V/m$ and $2.0\mu V/m$ for $T_e = 1000K$ and $T_e = 5000K$, respectively, when the e-folding distance of density dropout along the filed lines was 200 km. For ions, steady-state motions exist in the ionosphere in the altitudes where ion-neutral collision frequencies exceed ion acoustic wave frequencies. In that case, parallel motions can be written as [Kelley, 1989],

$$V_{i//} = b_i E_{//} - D_i \frac{\nabla_{//} n}{n} - \frac{g}{\nu_{in}}. \qquad (6)$$

Here, b_i and D_i denote mobility and diffusion coefficient of ions defined by $\frac{q_i}{M_i \nu_{in}}$ and $\frac{k_B T_i}{M_i \nu_{in}}$, respectively. Symbols, M_i, q_i, ν_{in}, and g are ion mass, electric charge of ions, ion-neutral collision frequency, and gravity, respectively. Ion-neutral collision frequencies from 400 km to 1000 km in altitudes were plotted in Figure 2 using nighttime sunspot maximum condition in Prince and Bostick (1964). Frequencies of ion acoustic wave were calculated by substituting wavelength of ion acoustic wave into the dispersion relation. The wavelength was assumed to be identical to initial accumulation distance along the field lines. We chose two cases, 1000 km and 4000 km. Phase velocity of the ion acoustic wave of the order of 1600 m/s for the electron temperatures of 5000K yields the wave frequencies of $1.6 \times 10^{-3} s^{-1}$ for the wavelength of 1000 km and $4.0 \times 10^{-4} s^{-1}$ for 4000 km. These frequencies were overlaid in Figure 2. Steady-state ion motions can be adopted up to 800 km, for a wavelength over 1000 km.

Altitude profile of steady-state ion flows were evaluated substituting 1000K for ion temperatures and the same e-folding distance in equation (5). Ions are oxygen and parallel electric fields are given by the equation (5). Snapshot of the velocity profile in altitudes from 400 km to 800 km is shown in Figure 3 for the two cases of electron temperatures, 5000K for black dots and 1000K for red dots. For the low temperature case (1000k), there occurred no ion upflow because the parallel electric fields could not overcome gravity. We suggest that electron temperatures over 2700K would be needed to excite ion upflow. When electron temperature was set to 5000K, ion velocity 15 m/s at 400 km in altitudes increased rapidly to 1369 m/s at 800 km. The altitude profile of the flow velocity in Figure 3 matched Type 2 ion outflow observed by EISCAT radar [Wahlund et al., 1992]. We conclude that the ion upflow in topside ionosphere was caused primarily by the parallel electric fields excited by the upward travelling ion acoustic wave. Below 600 km in altitudes, upflow velocity was one-to-two orders of magnitudes smaller than the equatorward drift in the flow channel. Upflow velocity became comparable to the horizontal drift over 800 km in altitudes and exceeded the phase velocity of ion acoustic wave. Parallel velocity that prevailed the ion acoustic phase velocity may excite a shock at the topside ionosphere. The shock velocity may increase with altitudes in higher electron temperatures. A part of them would be observed as electrostatic shock or double layers at the altitudes of 6000 – 8000 km [Mozer et al., 1976; Temerin et al., 1982]. Those electrostatic shocks would have produced parallel potential structures referred to as inverted-V at the low latitude end of the flow channel. In this scenario, inverted-V as well as upward FACs are major components contributing to auroral acceleration in lower latitudes.

5. Nonlinear evolution of the horizontal flows

Accumulation of electrons and ions occurred at the equatorward end of the flow channel. We can estimate a rate of accumulation by the following relation,

$$\frac{\Delta n}{\Delta t} = -n_0 \frac{\Delta U}{\Delta x}. \qquad (7)$$

Here n is plasma density, U denotes drift velocity in the flow channel in x. Substituting

$\Delta U = 10^3 ms^{-1}$ and $\Delta x = 10^4 m$, we have $\frac{\Delta n}{\Delta t} = 10^{10} m^{-3} s^{-1}$ for the background density $n_0 = 10^{11} m^{-3}$. This gives density pileup of the order of $\frac{\Delta n}{n_0} = 100\%$ in ten seconds. If the equatorward drift in the flow channel is an order of 10^3 m/s (E=100 mV/m in auroral ionosphere) and electron production by the precipitation do not exceed the accumulation rate which was 100% of the background density in ten seconds, both outflows and precipitation may not bring significant changes to the flux carried by $E \times B$ drift in the flow channel. We then approximate one dimensional (along the drift path in *x*) conservation equation in the flow channel.

$$\frac{\partial n}{\partial t} + \frac{\partial}{\partial x}(nU) = 0 \qquad (8)$$

A question arises regarding maximum accumulation of plasmas at the equatorward end of the flow channel because unlimited accumulation may not occur. One possible mechanism to suppress the accumulation may be associated with the ionospheric screening that decreased the amplitudes of penetrated (total) westward electric fields by the increasing ionospheric conductivities. In a two-dimensional ionosphere with uniform height-integrated conductivity, total electric fields *E* given by a sum of the incident (E_i) and reflected westward electric fields may be written as $E = \left(2\Sigma_A / \left(\Sigma_A + \Sigma_P\right)\right) E_i$, where Σ_A and Σ_P are Alfven conductance defined by $1/\mu_0 V_A$ and height-integrated Pedersen conductance in the ionosphere, respectively [Kan et al., 1982]. Symbols μ_0 and V_A denote magnetic permeability in vacuum and Alfven velocity, respectively. Amplitude ratio of total electric fields to incident electric fields is a function of conductance ratio of Pedersen and Alfven; $E/E_i = 2$ for a low conductivity of the ionosphere satisfying $\Sigma_P/\Sigma_A << 1$, and $E/E_i = 0$ for a high conductivity of the ionosphere satisfying $\Sigma_P/\Sigma_A >> 1$. Noting that Σ_P is proportional to the plasma density in the ionosphere, the total electric fields monotonically decreased with increasing plasma densities caused by accumulation itself and by the precipitations associated with the auroral activity. Another explanation may be suggested in the polarization electric fields (eastward) produced by the accumulation itself. These electric fields grew quickly with density accumulation and decreased the incident electric fields (westward) by the superposition. In addition to the above scenarios, we surmise that excess accumulation of the ionospheric plasmas may be suppressed through the term, $(\mathbf{U}\cdot\nabla)\mathbf{U}$, in the equation of motion. From the ionospheric screening process discussed above, we tentatively assume that flow velocity U is a function of the density n. Then the conservation equation (8) may be written as,

$$\frac{\partial n}{\partial t}+\frac{\partial}{\partial x}Q(n)=0\,. \qquad (9)$$

Here, $Q(n)$ is a mass flux defined by $Q(n)=nU(n)$. This relation can be reduced to nonlinear wave equation,

$$\frac{\partial n}{\partial t}+c(n)\frac{\partial n}{\partial x}=0\,. \qquad (10)$$

Here $c(n)$ is a wave propagation velocity defined by $c(n)=U(n)+nU'(n)$, $U(n)$ is a drift velocity in the flow channel, and $U'(n)$ denotes braking/acceleration of the drift velocity by increasing and decreasing density. The equation (10) is often referred to as propagation of "kinematic waves" to describe traffic flow [Lighthill and Whitham, 1955]. In the following, we use dimensionless units normalized by U_m, and n_m. Here, U_m and n_m denote maximum drift velocity at n=0 and maximum density for complete stops of the drift, respectively. Assuming a constant braking in the flow channel, we define U by a linear function of density n as $U(n)=1-n$. Noting that $Q'(n)=c(n)$, this relation is reduced to the equation, $Q(n)=n(1-n)$, identical to the case for the traffic flow [Whitham, 1999]. Both the *U and Q* are plotted in Figure 4A as a function of *n*. A nonlinear evolution of the waves is presented in Figure 4B by the characteristic curves. In the case of vehicles in traffic, the initial flows started from n=0 and stopped at n=1.0 by the tailback of cars. For the case of the ionosphere, the ionospheric density started from a finite density, n=0.3 (Figure 4B), and increased to n=1.0 to terminate the flow by the full screening. The nonlinear evolution of the density profile in time is shown in Figure 4B in colors from black ($T=T_1$), red ($T=T_2$), green ($T=T_3$), blue ($T=T_4$), and to purple ($T=T_5$). After $T=T_5$, the waves propagate upstream (poleward) as a shock. The shock velocity, V, is given as [Whitham, 1999],

$$V = \frac{Q(n_2) - Q(n_1)}{n_2 - n_1}. \qquad (11)$$

Here, subscript 1 is for the values ahead shock and subscript 2 is for the values behind. Noting that $Q(n_2)=0$ and substituting $Q(n_1)=n_1(n_2-n_1)$, the equation (11) can be reduced to $V = -n_1$ in dimensionless unit. The propagation velocity of the shock is related to the densities ahead. For the case of n=0.3 in Figure 4B, shock velocity can be estimated to be -0.3U_m. Here, U_m denotes maximum drift velocity in the ionosphere where ionospheric screening effects vanished by the condition, $\Sigma_P / \Sigma_A << 1$.

We employed the traffic flow analogy to explain the poleward expansion of auroras. A similar case may be found in “flow braking in near-Earth tail” [Shiokawa et al., 1997]. In this case, the advective term in the equation of motion suppressed an excess pileup of the pressures caused by the fast earthward flow itself. This may minimize the velocity of the ion flows at the pressure peak analogous to a tailback of cars in traffic flows.

6. Summary

Allowing for the compressibility of the ionosphere caused by the ionospheric drifts of the order of kilometers per second, we proposed a new scenario for the poleward expansion of auroras including generation of field-aligned currents and parallel electric fields of the ionospheric origin. This scenario, analogous to a traffic flow of cars on the crowded roads, partly explains the discrepant time history of the auroras which is often described as the auroras expand opposite to that of plasma drift in the ionosphere.

Acknowledgements

The author would like to express his sincere thanks to all the members of Global Aurora Dynamics Campaign (GADC) [Oguti et al., 1988]. We also gratefully acknowledge STEP Polar Network (http://step-p.dyndns.org/~khay/). Geomagnetic coordinates and footprints of the satellites

are available at the Data Center for Aurora in NIPR (http://polaris.nipr.ac.jp/~aurora)

References

Akasofu, S.-I., Kimball, D.S., and Meng, C.-I.: Dynamics of the aurora-VII, Equatorward motions and the multiplicity of auroral arcs, J.Atmos.Terr.Phys., 28, 627-635, 1966.

Chen, F.F.: Introduction to plasma physics, Plenum Press, New York, 1974.

Haerendel, G.: Plasma drifts in the auroral ionosphere derived from Barium release, in Earth magnetospheric processes, B.M. McComac (ed), D.Reidel Publishing Company, 246-257, 1972.

Kadomtsev, B.B,: Collective phenomena in plasmas (in Japanese), Iwanami shoten, Tokyo, 1976.

Kan, J.R., Longenecker, D.U., and Olson, J.V.: A transient response of Pi2 pulsations, J.Geophys.Res., 87, 7483-7488, 1982.

Kelley, M.C., Starr, J.A., and Mozer, F.S.: Relationship between magnetospheric electric fields and the motion of auroral forms, J.Geophys.Res., 76, 5256-5277, 1971.

Kelley, M.C.: The earth’s ionosphere: plasma physics and electrodynamics, Academic Press, Inc., 1989.

Lighthill, M.J., and Whitham, G.B.: On kinematic waves. II. A theory of traffic flow on long crowded roads, Proc. R. Soc. Lond. A, 229, 317-345, 1955.

Mozer, F.S., Carlson, C.W., Hudson, M.K., Torbert, R.B., Parady, B., Yatteau, J., and Kelley, M.C.: Observations of paired electrostatic shocks in the polar magnetosphere, Phys.Rew.Lett., 38, 292-295, 1977.

Nielsen, E., and Greenwald, R.A.: Variations in ionospheric currents and electric fields in association with absorption spikes during substorm expansion phase, J.Geophys.Res., 83, 5645-5654, 1978.

Oguti, T., Kitamura, T., and Watanabe, T.: Global aurora dynamics campaign, 1985-1986, J.Geomag.Geoelectr, 40, 485-504, 1988.

Oguti, T.: Introduction to auroral physics (in Japanese), Laboratory for Solar-Terrestrial Environment, Nagoya University, 2010.

Prince, Jr., C.E., and Bostick, Jr., F.X.: Ionospheric transmission of transversely propagated plane waves at micropulsation frequencies and theoretical power spectrums, 69, 3213-334, 1964.

Radoski, H.R.: Highly asymmetric MHD resonances: The guided poloidal mode, J.Geophys.Res., 72, 4026-4027, 1967.

Rubtsov, A., Mager, P.N., and Klimushkin, D.Yu.: Ballooning instability of azimuthally small scale coupled Alfven and slow magnetoacoustic modes in two-dimensionally inhomogeneous magnetospheric plasma, Phys.Plasmas, 25, doi:10.1063/1.5051474, 2018.

Runov, A., Angelopoulos, V., Zhou, X.-Z., Zhang, X.-J., Li, S., Plaschke, F., and Bonnell, J.: A THEMIS multicase study of dipolarization fronts in the magnetotail plasma sheet, J.Geophys.Res., 116, A05216, doi:10.1029/2010JA016316, 2011.

Saka, O., Akaki, H., Reeves, G.D., and Baker, D.N.: Magnetic fields and particle signatures in the vicinity of nightside geosynchronous altitudes in the first one-minute-interval of Pi2 onset: a case study, J.Atomos.Solar Terr.Phys., 62, 17-30, 2000.

Saka, O., Koga, D., and Hayashi, K.: A plasma bulk motion in the midnight magnetosphere during auroral breakup inferred from all-sky image and magnetic field observations at geosynchronous altitudes. J.Atomos.Solar Terr.Phys. 69, 1063-1074, 2007.

Saka, O. Hayashi, K, and Thomsen, M.: First 10 min intervals of Pi2 onset at geosynchronous altitudes during the expansion of energetic ion regions in the nighttime sector, J.Atmos.Solar Terr.Phys., 72, 1100-1109, 2010.

Saka, O., Hayashi, K., and Koga, D.: Periodic aurora surge propagating eastward/westward at poleward boundary of aurora zone during the first 10 min intervals of Pi2 onset, J.Atmos.Sol. Terr.Phys., 80, 285-295, doi:10.1016/j.jastp.2012.02.010, 2012.

Saka, O., Hayashi, K., and Koga, D.: Excitation of the third harmonic mode in meridian planes for Pi2 in the auroral zone, J.Geophys.Res., 117, doi:10.1029/2012JA018003, 2012.

Saka, O., Hayashi, K., and Thomsen, M.: Pre-onset auroral signatures and subsequent development of substorm auroras: a development of ionospheric loop currents at the onset latitudes, Ann. Geophys., 32, 1011-1023, 2014.

Saka, O., Hayashi, K., and Leonovich, A.S.: Explanation of Pi2 pulsations in auroral zone: Azimuthal propagation of ionospheric loop currents, J.Geophys.Res., 120, doi:10.1002/2015JA021128, 2015.

Saka, O., and Hayashi, K.: Longitudinal expansion of field line dipolarization, J.Atomos.Solar Terr.Phys., 164, 235-242, 2017.

Shiokawa, K., Baumjohann, W., and Haerendel, G.: Braking of high-speed flows in the near-Earth tail, Geophys.Res.Lett, 24, 1179-1182, 1997.

Temerin, M., Cerny, K., Lotko, W., and Mozer, F.S.: Observations of double layere and solitary waves in the auroral plasma, Phys.Rew.Lett., 48, 1176-1179, 1982.

Tsyganenko, N.A.: A magnetospheric magnetic field model with a warped tail current sheet. Planet. Space Sci., 37, 5-20, 1989.

Wahlund, J.-E., Opgenoorth, H.J., Haggstrom, I., Winser, K.J., and Jones, G.O.: EISCAT observations of topside ionospheric outflows during auroral activity: revisited, J.Geophys.Res., 97, 3019-3017, 1992.

Whitham, G.B.: Linear and nonlinear waves, A Wiley-Interscience Publication, JOHN WILEY & SONS, INC., 1999.

Figure Captions

Fig. 1: Vertical profiles from 90 km to 1000 km in altitudes of electron number density in two conditions, pre-onset in black and after accumulation in red. Nighttime sunspot maximum condition given in Prince and Bostic (1964) was used to plot pre-onset condition. Vertical arrows directing upward and downward denote travelling ion acoustic waves propagating along the field lines from the density peak of F layer.

Fig.2: Ion-neutral collision frequency (ν_{in}) in altitudes from 400 km to 1000 km calculated using nighttime sunspot maximum condition in Prince and Bostick (1964). Wave frequencies of ion acoustic wave are overlaid for two wavelength, 1000 km and 4000 km along field lines (see text).

Fig. 3: Steady-state parallel velocity in altitudes for ions (oxygen) produced by parallel electric fields $0.4\mu V/m$ (T_e=1000K) in red dots and $2.0\mu V/m$ (T_e=5000K) in black dots. Vertical flows in altitudes from 400 km to 800 km are shown. Flow velocity is positive upward and negative downward.

Fig. 4: (A) Normalized flux(Q)-density(n) curve (thin curve) and velocity(U)-density(n) line (thick line) in flow channel. Vertical scale of U-n line is shown to the right, scale of Q-n curve is to the left. Dotted line at n=0.5 indicates the critical density where $c(n)$ vanishes; waves are stationary relative to the ground. Waves propagate forward/backward at a density below/above the critical density. (B) Nonlinear evolution of the density accumulation. Density increased in a step like manner from T_1 to T_5. Shock velocity is 1.2 km/sec poleward when U_m=4.0 km/s is assumed at n=0.3 (see text).

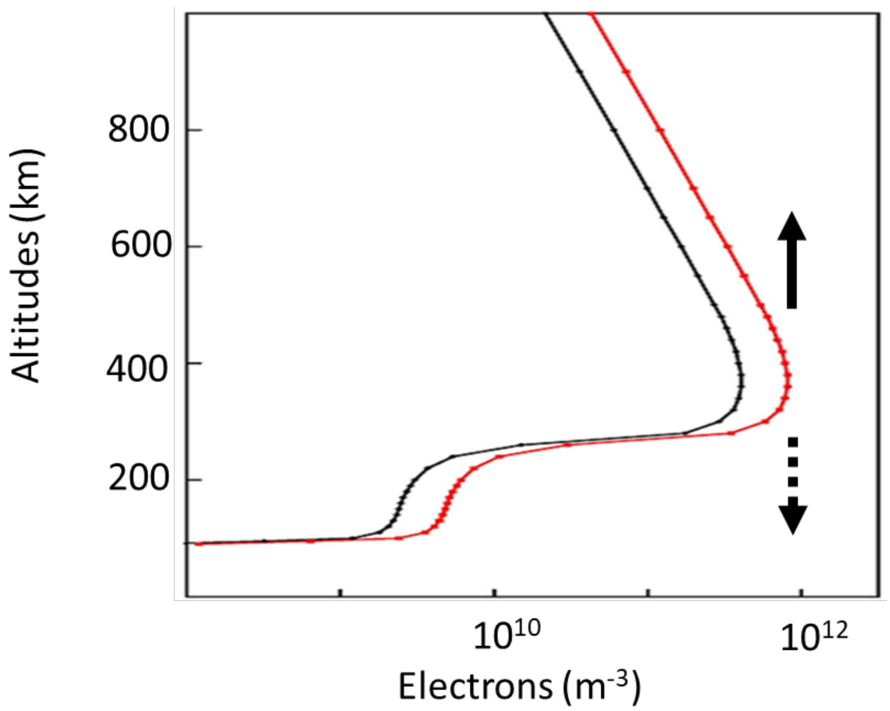

Figure 1

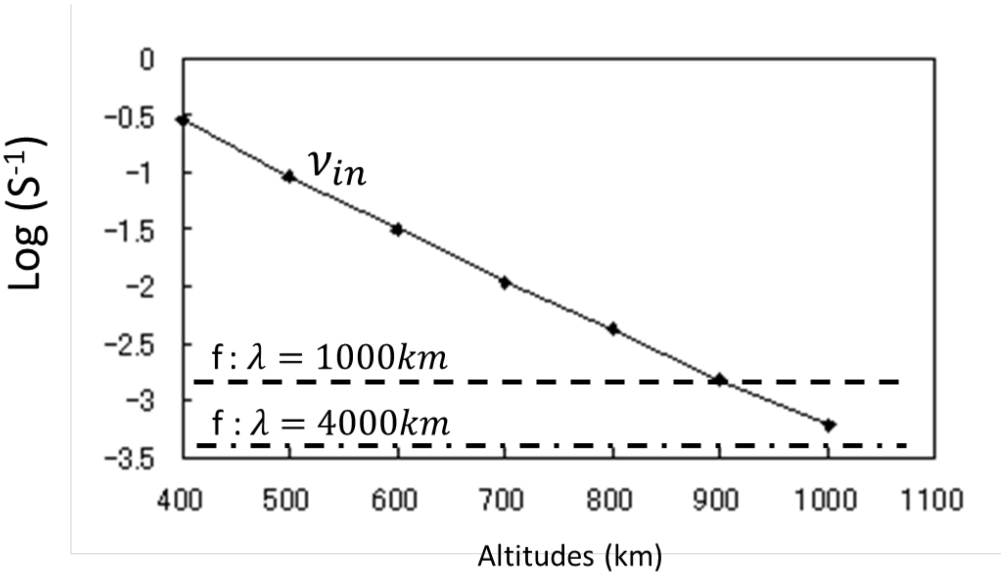
0
-0.5
-1
-1.5
-2
-2.5
-3
-3.5
Log (S-1)
ν_{in}
f : $\lambda = 1000km$
f : $\lambda = 4000km$
400
500
600
700
800
900
1000
1100
Altitudes (km)

Figure 2

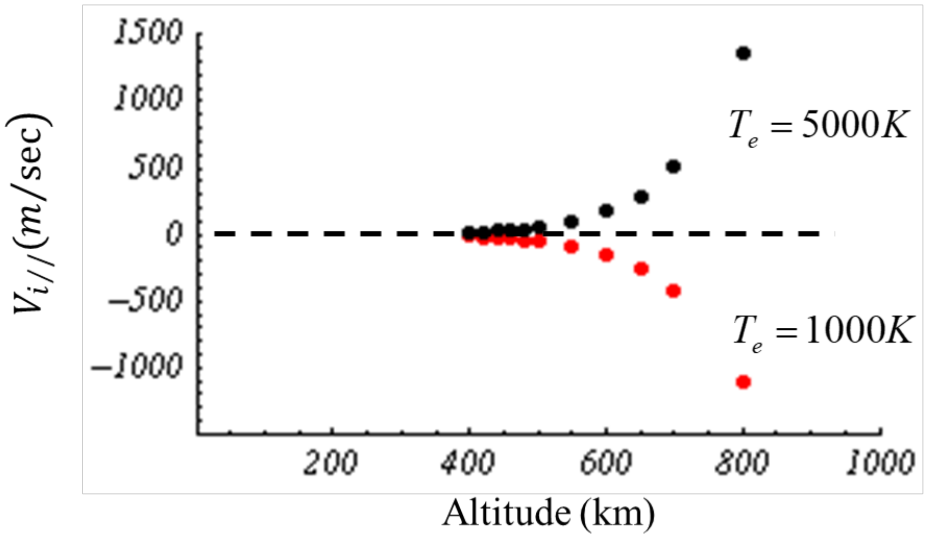

1500
1000
500
0
−500
−1000
200
400
600
800
1000
$V_{i//}(m/sec)$
$T_e = 5000K$
$T_e = 1000K$
Altitude (km)

Figure 3

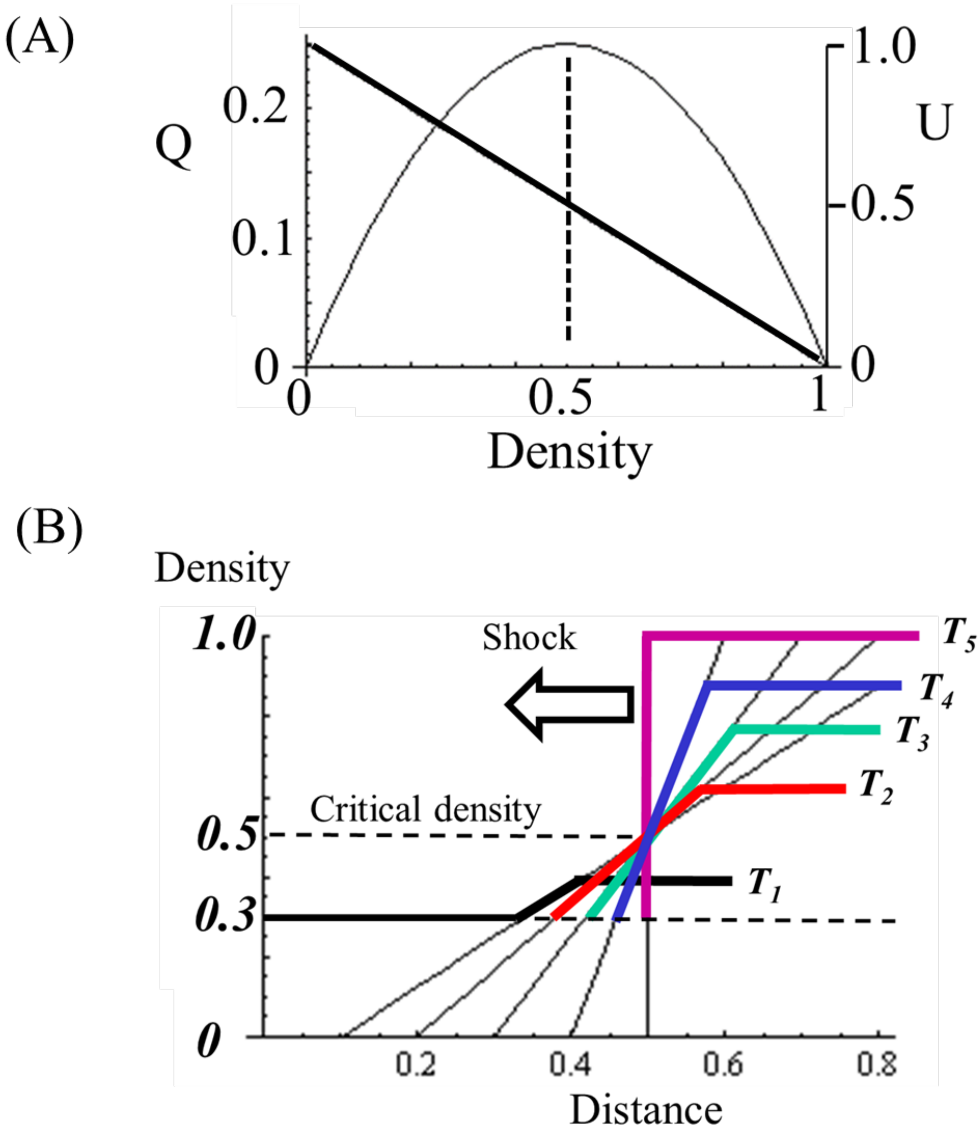

(A)
Q
0.2
0.1
0
0
0.5
1
Density
1.0
U
0.5
0
(B)
Density
1.0
Shock
T_5
T_4
T_3
Critical density
T_2
0.5
T_1
0.3
0
0.2
0.4
0.6
0.8
Distance

Figure 4